J Mater Sci (2011) 46:3101–3107
DOI 10.1007/s10853-010-5189-6

Use of recalescence behavior analysis for the prediction of grain refinement in undercooled Cu–Ni alloy

W. Yang · F. Liu · Z. F. Xu · B. P. Lu · G. C. Yang

Received: 5 November 2010 / Accepted: 10 December 2010 / Published online: 29 December 2010

Abstract Considering non-equilibrium solidification and its influence on subsequent near-equilibrium solidification together, the description of recalescence behavior in bulk undercooled $Cu_{70}Ni_{30}$ alloy was adopted to predict the corresponding microstructure transition. The thermal plateau time for near-equilibrium solidification can be deduced directly with the calculation of non-equilibrium solid fraction formed in recalescence. On the basis of quantitative description for recalescence behavior, the non-equilibrium solid fraction, residual liquid fraction, dendrite broken-up time, and thermal plateau time can be determined as functions of initial undercooling. Then, a simple and accurate application of dendrite fragmentation model was performed as the grain refinement at both low- and high-undercooling originates from dendrite breakup. The predicted undercooling regions for the double grain refinement agree well with the experimental observation. Moreover, the change of grain morphology for the second grain refinement can be ascribed to the occurrence of recrystallization produced by the enhanced residual stress upon highly undercooled solidification.

W. Yang (✉) · Z. F. Xu · B. P. Lu
National Defence Key Discipline Laboratory of Light Alloy Processing Science and Technology, Nanchang Hangkong University, Nanchang 330063, People's Republic of China
e-mail: weiyang@mail.nwpu.edu.cn

F. Liu · G. C. Yang
State Key Laboratory of Solidification Processing, Northwestern Polytechnical University, Xi'an 710072, Shaanxi, People's Republic of China

Introduction

The formation of refined grain structure is a subject of great interest in metallurgy and materials science because of improved mechanical properties for polycrystalline materials [1]. Generally, grain refinement can be achieved by adding certain micron-sized particles to melts due to the enhancement of nucleation rate [2, 3]. Since the first observation of grain refinement in undercooled pure Ni by Walker [4], this phenomenon has been detected universally in many metallic systems (e.g., Fe–Co [5], Fe–Ni [6], Ni–C [7], and Ni–Cu [8, 9]) using different rapid solidification techniques (e.g., melt fluxing [5, 6], electromagnetic levitation [9], drop-tube [10], and melt-spun [11]). Moreover, it was also found that this unique grain refinement can occur not only at high undercooling, but also at low undercooling [9, 10]. Compared with the conventional method by mechanical stirring or adding particles to the melts, the characteristic transition from coarse dendrite to grain-refined microstructure in undercooled liquid is intrinsic to the process itself.

In order to achieve a better understanding of this phenomenon, investigations have been performed extensively and different mechanisms were proposed separately, including dynamic nucleation [4], critical growth velocity which assumes that the grain refinement is accompanied by the abrupt transition in velocity and undercooling curve [12], kinetics induced growth instabilities [13–15], recrystallization [16], dendrite remelting [17], and dendrite fragmentation [18, 19]. Then, the model suggested by Karma has been widely accepted, which assumes that the grain refinement originates from dendrite fragmentation due to Rayleigh instabilities and occurs when the thermal plateau time following recalescence Δt_{pl} exceeds the dendrite break-up time Δt_{bu} [18]. Applying this criterion, the

predicted grain refinement regions agree well with the observed results in electromagnetic levitation and drop tube experiments [8, 9].

As suggested in Karma's model [18, 19], the dendrite break-up time Δt_{bu} can be quantitatively calculated as a function of dendrite trunk radius R, which is dependent of initial undercooling ΔT and proportional to the dendrite tip radius R_{tip} deduced from dendrite growth model. However, the thermal plateau time Δt_{pl} is estimated roughly from the experimental cooling curve, which brings uncertainty and inconvenience to the model application.

Actually, solidification of bulk undercooled liquid is composed of two successive regimes, i.e., rapid solidification accompanying recalescence and the subsequent near-equilibrium solidification during which the residual liquid crystallizes continuously [20]. Therefore, it can be believed that the formation of grain refinement microstructure is caused by the specific transformation experience of the above two processes. Moreover, the fragmentation model is proposed for post-recalescence stage, which is controlled by the combination of residual liquid fraction and heat extraction rate to environment [18, 19]. It can be concluded that the duration of thermal plateau stage should be determined by the previous rapid solidification process and the as-formed non-equilibrium solid fraction f_s, rather than considering this period alone. In our previous work [21–23], the recalescence behavior of bulk undercooled melts has been described quantitatively with the calculation of liquid/solid Gibbs free energy by assuming thermal balance and solute conservation. Because of the advantage of unlimited miscibility for studying the effect of solidification without being affected by subsequent phase transformations, $Cu_{70}Ni_{30}$ alloy was chosen and the predicted maximal recalescence temperature T_R agrees well with the experimental results [22].

The purpose of this article is to derive a quantitative link between the non-equilibrium solidification and the subsequent near-equilibrium solidification, where the thermal plateau time for the latter stage can be calculated according to the solid fraction formed in the former stage using the predicted maximum recalescence temperature. On this basis, the analysis of these two transformation processes is further applied to interpret the corresponding microstructure evolution, which gives a more accurate prediction of grain refinement regions and better explanation of grain morphological transition for bulk undercooled Cu–Ni alloy.

Experimental procedure

The undercooling experiments were performed by melt fluxing method. The flux agent, i.e., analytical pure (AP) grade boron oxide, was used after having been fully dehydrated in an electro-resistant furnace at 1073 K for 8 h. The experimental apparatus consists of a high-frequency induction heating facility, an infrared pyrometer and a signal recorder. $Cu_{70}Ni_{30}$ alloy with a mass of 5 g was in situ melted from high-purity elements of nickel (Ni) and copper (Cu) better than 99.98 wt%. Prior to melting, the surfaces of the metal charges were cleaned mechanically by grinding off the surface oxide layer and chemically by etching in HCl solution diluted by alcohol. In order to obtain undercooling as large as possible, the superheating–cooling procedure was repeated between two and five times so as to vary the nucleation capacity of the heterogeneous catalyst by decomposition, melting, or passivation effect prior to crystallization. After the sample had been superheated to the desired temperature for 3–10 min, the induction heater was turned off so that the sample was spontaneously cooled down to room temperature. The heating and cooling curves of the melts were in situ measured by an infrared pyrometer, which was calibrated with a standard PtRh30-/PtRh6 thermocouple, and had an accuracy of 3 K, and a response time less than 5 ms.

After experiment, the solidified samples were sectioned longitudinally and processed according to standard metallographic procedure. The microstructure observation was performed using a PMG3 Olympus optical microscope and the dendrite length and spherical grain diameter were determined by the linear intercept method.

Results and discussion

Microstructure evolution with undercooling

Figure 1 shows the as-solidified microstructure morphologies of $Cu_{70}Ni_{30}$ alloy subject to different undercoolings. If solidification occurs at the undercooling of 20 K, coarse dendrites with well-developed primary trunks and secondary arms form primarily (Fig. 1a). This can be ascribed to the rapid propagation of formed dendrite to the volume of melts once upon the onset of nucleation and the suppression of further nucleation due to its released fusion heat. Subsequently, as the undercooling increases to 44 and 90 K, these coarse dendrites transform to quasi-spherical grains, and the first spontaneous grain refinement phenomenon occurs, which can be inferred from the abrupt decrease of grain size shown in Fig. 1b and c in comparison with that in Fig. 1a. However, dendrite morphology appears again with the undercooling of 123 K and grows into the undercooled melt undergoing a preferred growth transient zone after the start of nucleation (Fig. 1d). This can be inferred from the highly branched directional and fine patterns in the overall cross-section in comparison to that for 20 K undercooling.

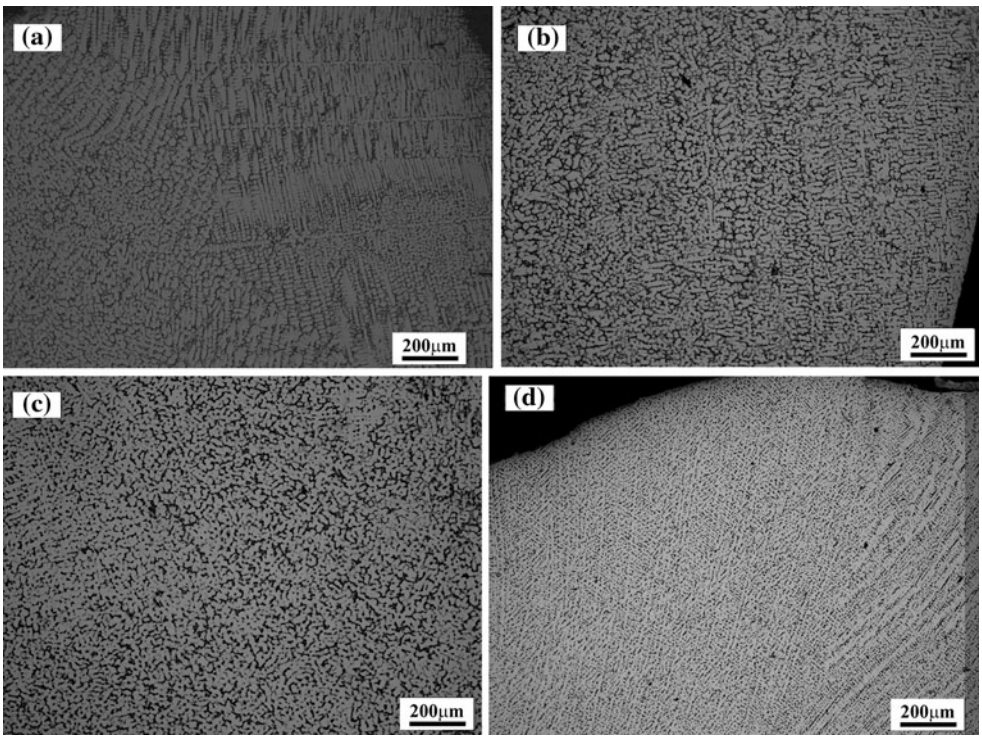

Fig. 1 As-solidified microstructures of $Cu_{70}Ni_{30}$ alloy at small undercooling: **a** $\Delta T = 20$ K; **b** $\Delta T = 44$ K; **c** $\Delta T = 90$ K; **d** $\Delta T = 123$ K

As undercooling rises up to 158 K, some of the primary dendrite arms begin to detach from its trunk (Fig. 2a), while the dendritic structure remains predominant. This effect is further strengthened for $\Delta T = 186$ K, where the directionally thin dendrite has been broken into small pieces, indicating the occurrence of second grain refinement (Fig. 2b). For undercooling of 220 and 256 K, refined grains form completely with the large increase of grain number (Fig. 2c, d).

However, it is worth noting that there are quite different characteristics between the second refined structures with different undercoolings. This can be inferred from the enlarged pictures for $\Delta T = 220$ and 256 K shown in Fig. 3. As can be seen clearly, the refined grain for $\Delta T = 220$ K presents granular morphology with smooth grain boundary and uniform grain size, which is similar to the first refinement phenomenon (Fig. 3a). In contrast, the as-solidified structure for $\Delta T = 256$ K is composed of hexagonal equiaxed grains with straight and flat edges, accompanying the abnormal large grains coexisting with fine equiaxed grains (Fig. 3b).

Based on the above analysis, the grain size as a function of ΔT for $Cu_{70}Ni_{30}$ alloy is plotted in Fig. 4. Obviously, two grain refinement regimes occur within the range of undercooling examined here. With the decrease of grain size from $\sim$1700 μm to less than 25 μm, the first grain refinement takes place and remains in the lower undercooling, i.e., $44\ \text{K} < \Delta T < 90$ K. The second occurs at $\Delta T > 200$ K, indicated by the reduction of grain size from $\sim$3000 μm to less than 50 μm again.

Relations between non-equilibrium and near-equilibrium solidification stages

As mentioned above, the occurrence of grain refinement can be explained by the dendrite fragmentation model with the comparison of dendrite break-up time and thermal plateau time. As the thermal plateau stage is associated with the amount of solid fraction formed in non-equilibrium solidification process, its duration time can be determined from the recalescence extent, as well as the maximum recalescence temperature, without resorting to experimental estimation. According to the energy conservation principle, the thermal plateau time Δt_{pl} can be calculated as [8]:

$$\Delta t_{\text{pl}} = \frac{f_{\text{l}}\Delta H}{C_{\text{p}}\Phi} = \frac{(1 - f_{\text{s}})\Delta H}{C_{\text{p}}\Phi}, \tag{1}$$

where f_{l} is the residual liquid fraction after recalescence, ΔH is the fusion heat, C_{p} is the heat capability of liquid, and Φ is the liquid cooling rate and was chosen as 14 K/s in the current experiment [22].

Assuming the solidification within recalescence to be an adiabatic process, the non-equilibrium solid fraction formed in this period is proportional to the temperature rising during recalescence, ΔT_{R}, and can be expressed as [24]:

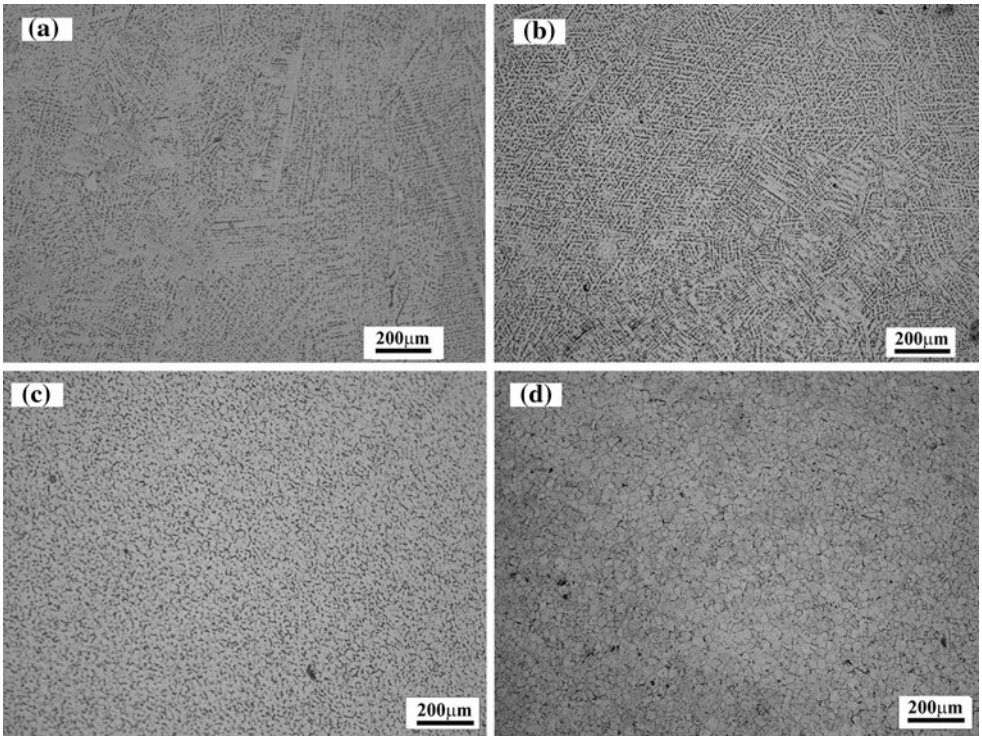

Fig. 2 As-solidified microstructures of $Cu_{70}Ni_{30}$ alloy at large undercooling: **a** $\Delta T = 158$ K; **b** $\Delta T = 186$ K; **c** $\Delta T = 220$ K; **d** $\Delta T = 256$ K

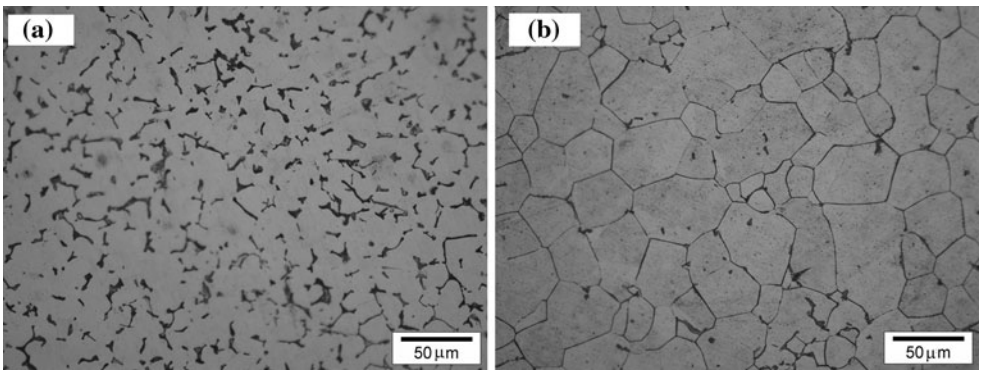

Fig. 3 High-magnification microstructure morphologies of $Cu_{70}Ni_{30}$ alloy for second grain refinement: **a** $\Delta T = 220$ K; **b** $\Delta T = 256$ K

$$f_s = \frac{\Delta T_R C_p}{\Delta H} = \frac{(T_R + \Delta T - T_l)C_p}{\Delta H}, \quad (2)$$

where T_l is the liquidus temperature.

Applying thermal balance and solute conservation principles, a numerical model was proposed to describe the recalescence behavior of bulk undercooled melts with the quantitative calculation of liquid/solid Gibbs free energy. Detailed information was given in Refs. [21, 22]. Figure 5 shows the predicted maximum recalescence temperature T_R and the corresponding ΔT_R as functions of undercooling. With the increase of ΔT, the maximum recalescence temperature decreases continuously and deviates from its liquidus temperature significantly. However, the recalescence extent increases gradually due to the enhanced non-equilibrium effect. Incorporating Eq. 2 and the results in Figs. 5 and 6 present the evolution of non-equilibrium solid fraction as a function of undercooling. Analogous to that for ΔT_R, f_s increases with ΔT in a linear like manner.

Comparison of theoretical analysis with experimental observation

According to dendrite fragmentation model [18, 19], the dendrite break-up time can be calculated by the following equation:

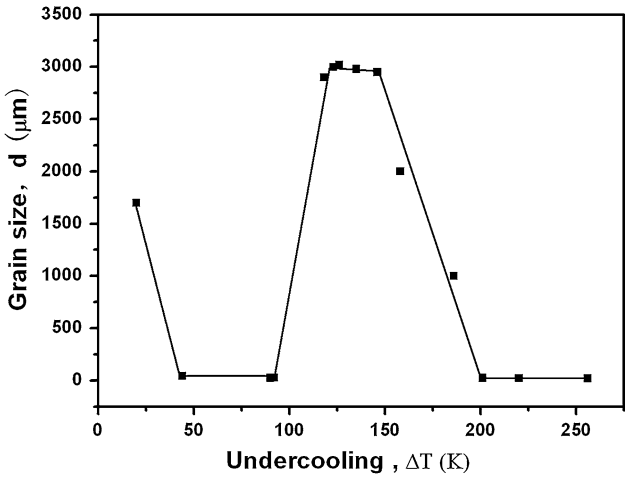

Fig. 4 Measured grain size as a function of undercooling for the undercooled $Cu_{70}Ni_{30}$ alloy

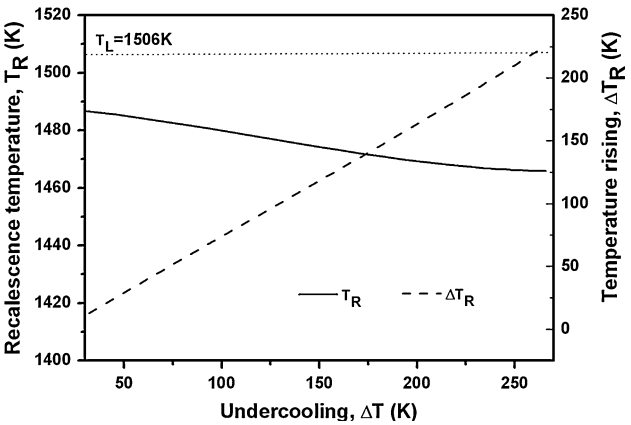

Fig. 5 Predicted maximum recalescence temperature and recalescence extent as functions of undercooling for the undercooled $Cu_{70}Ni_{30}$ alloy

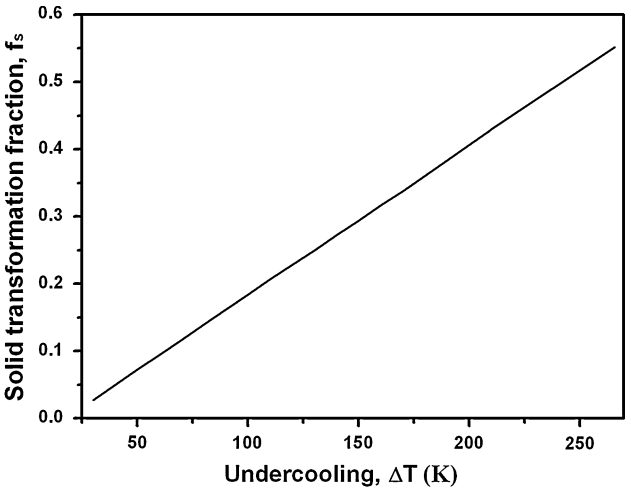

Fig. 6 Non-equilibrium solid fraction as a function of undercooling for the undercooled $Cu_{70}Ni_{30}$ alloy

$$\Delta t_{bu}(\Delta T) \approx \frac{3}{2}\frac{R(\Delta T)^3}{d_0 D_T}\left|1+\frac{|m_l C_0(1-k_e)D_l|}{\Delta H_f/C_p \quad D_T}\right| \tag{3}$$

with m_l as the equilibrium liquidus slope, k_e the equilibrium segregation coefficient, d_0 ($=\Gamma C_p/\Delta H$) the capillary length, and Γ the Gibbs–Thomson coefficient. The dendrite trunk radius R, as a function of ΔT, is correlated to dendrite tip radius R_{tip} with a scaling factor of 20 [18, 19]. Analogous to previous study [25, 26], the stability constant in dendrite growth model was herein chosen as $1/4\pi^2$ for the sake of simplicity. Actually, it may vary with the crystal anisotropy, alloy composition, undercooling, and the ratio of thermal diffusivity D_T to solute diffusivity D_l in liquid [27–29].

Using the basic physical parameters for $Cu_{70}Ni_{30}$ listed in Table 1 [12, 17, 22], Fig. 7 shows the variations of Δt_{pl} and Δt_{bu} as functions of undercooling calculated by Eqs. 1 and 3 separately. As can be seen clearly, there are three intersections of the two curves at 32, 106, and 181 K, respectively. According to dendrite fragmentation model, there is double grain refinement when 32 K $< \Delta T <$ 106 K and $\Delta T >$ 181 K, in which break-up occurs before the sample has enough time to solidify completely, i.e., $\Delta t_{pl} > \Delta t_{bu}$. In other cases, coarse dendrites will not break up because of insufficient time. In comparison with the above experimental observation and the reported results [8, 30], the model prediction is satisfactory.

Also, it is necessary to follow the morphological change in the second refinement region. For smaller undercooling, the observed spherical-shaped grains originate from the fragmentation of primary dendrites and their side-branches. As mentioned above, the refined grain at larger undercooling is different with that at smaller undercooling (Fig. 3), which may be ascribed to recrystallization. From Fig. 6, it can be seen that the solid fraction formed in non-equilibrium transformation stage increases with undercooling, which leaves less residual liquid in the subsequent near-equilibrium solidification process. In such a case, the formed dendrites connect together and form a mesh

Table 1 Physical parameters for the $Cu_{70}Ni_{30}$ alloy used in the model calculations [12, 17, 22]

Parameters		Unit	Values
Heat of solidification	ΔH_f	J/kg	231700
Specific heat	C_p	J/kg K	576
Capillarity constant	Γ	K m	2.627×10^{-7}
Liquidus temperature	T_l	K	1506
Thermal diffusivity in liquid	D_T	m^2/s	7.5×10^{-6}
Solute diffusivity in liquid	D_l	m^2/s	7×10^{-9}
Equilibrium liquidus slope	m_l	–	5.6
Equilibrium segregation coefficient	k_e	–	1.485

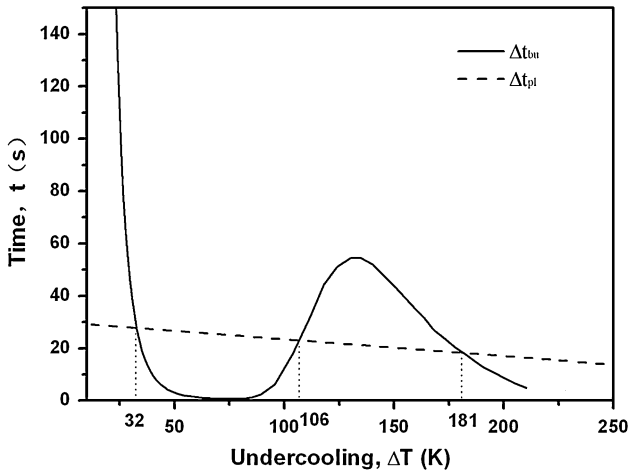

Fig. 7 Calculated Δt_{bu} and Δt_{pl} as functions of undercooling for the undercooled $Cu_{70}Ni_{30}$ alloy

structure, which generates larger resistance against the flowing of residual liquid and delays its compensation to the mushy zone of the sample. Consequently, the residual stress in the solidified solid is significant. Additionally, more solute atoms are trapped in the formed solid for larger undercooling, accompanying the enhanced dislocation and defects, which increase the distortional energy of crystal lattice. The combination of these effects provides the driving force for the subsequent recrystallization and forms the observed straight grain boundary. In local regions with relatively high-dislocation density and stress concentration, the recrystallized grain grows through merging with the surrounding grains, while the other grains grow normally. Consequently, abnormal large grain occurs and leads to non-uniform grain size distribution in the final microstructure.

Conclusions

Association of non-equilibrium solidification and the subsequent near-equilibrium solidification processes was constructed and further applied to predict the microstructure evolution for bulk undercooled $Cu_{70}Ni_{30}$ alloy. On the basis of quantitative description for recalescence behavior, the non-equilibrium solid fraction, residual liquid fraction, dendrite broken-up time, and thermal plateau time can be determined as functions of initial undercooling. With the comparison of dendrite broken-up time and thermal plateau time, the grain refinement phenomenon can be predicted by applying dendrite fragmentation model, giving excellent agreement with the experimental results. The analysis of the grain morphology transition for second grain refinement shows the occurrence of recrystallization because of the enhanced residual stress in larger non-equilibrium solid fraction for higher undercooling.

Acknowledgements W. Yang is grateful to the financial support by the fund of the State Key Laboratory of Solidification Processing in NWPU (SKLSP201118) and Scientific Starting Foundation for Doctorate Research in Nanchang Hangkong University (EA201003234). The authors are also grateful to the Free Research Fund of State Key Lab. of Solidification Processing (09-QZ-2008; 24-TZ-2009), the 111 project (B08040), the Natural Science Foundation of China (Grant nos. 50771084; 51071127, 50901059), National Basic Research Program of China (973 Program) 2011CB610403, the HuoYingdong Yong Teacher Fund (111052), the Fundamental Research Fund of Northwestern Polytechnical University (2008JC01), Aeronautical Science Foundation of China (2008ZF56016), the Open Fund of Aeronautical Science and Technology Key Lab. of Aeronautical Materials Processing in Nanchang Hangkong University and the Project of Education Department of Jiangxi (GJJ08199).

References

1. Christian JW (2002) The theory of transformation in metals and alloys, 3rd edn. Pergamon Press, Oxford
2. Kurz W, Fisher DJ (1998) Fundamentals of solidification, 4th edn. Trans Tech Publications Ltd, Switzerland
3. Baker JC, Cahn JW (1971) Solidification, 1st edn. ASM, Metals Park, OH
4. Walker JL (1959) The physical chemistry of process metallurgy. Wiley Interscience, New York, NY
5. Liu N, Liu F, Yang GC, Chen YZ, Chen D, Yang CL, Zhou YH (2007) Physica B 387:151
6. Chen YZ, Yang GC, Liu F, Liu N, Xie H, Zhou YH (2005) J Cryst Growth 282:490
7. Eckler K, Norman AF, Gätner F (1997) J Cryst Growth 173: 528
8. Han XJ, Yang C, Wei B, Chen M, Guo ZY (2001) Mater Sci Eng A 307:35
9. Girtneri F, Norman AF, Greer AL, Zambon A, Ramous E, Eckler K, Herlach DM (1997) Acta Mater 45:51
10. Norman AF, Eckler K, Zambon A, Gärtner F, Moir SA, Ramous E, Herlach DM, Greer AL (1998) Acta Mater 46:3355
11. Maslov VV, Nosenko VK, Jurisch M (2002) J Mater Sci 37:4663. doi:10.1023/A:1020668904024
12. Willnecker R, Herlach DM, Feuerbacher B (1990) Appl Phys Lett 56:324
13. Dragnevski K, Cochrane RF, Mullis AM (2002) Phys Rev Lett 89:215502
14. Mullis AM, Cochrane RF (1997) J Appl Phys 82:3783
15. Mullis AM, Cochrane RF (1998) J Appl Phys 84:4905
16. Powell GLF (1968) Trans Met Soc AIME 242:2133
17. Li JF, Zhou YH, Yang GC (2000) Mater Sci Eng A 277:161
18. Karma A (1998) Int J Non-Equilib Process 11:201
19. Schwarz M, Karma A, Eckler K (1994) Phys Rev Lett 73:1380
20. Liu F, Yang GC (2006) Int Mater Rev 51:145
21. Yang W, Liu F, Wang HF, Chen Z, Yang GC, Zhou YH (2009) J Alloys Compd 470:L13
22. Yang W, Liu F, Liu H, Yang GC, Zhou YH (2009) J Cryst Growth 311:3225
23. Yang W, Liu F, Wang HF, Chen Z, Yang GC, Zhou YH (2010) J Alloys Compd 491:118
24. Piccone TJ, Wu Y, Shiohara Y, Flemings MC (1987) Metall Trans A 18:925

25. Galenko PK, Danilov DA (1999) J Cryst Growth 197:992
26. Wang TM, Xu JJ, Xiao TQ, Xie HL, Li J, Li TJ, Cao ZQ (2010) Phys Rev E 81:042601
27. Rosam J, Jimack PK, Mullis AM (2008) Acta Mater 56:4559
28. Ramirez JC, Beckermann C (2005) Acta Mater 53:1721
29. Sha W, Wu X, Keong KG (2010) Electroless copper and nickel-phosphorus plating: processing, characterisation and modelling, 1st edn. Woodhead Publishing Limited, Cambridge
30. Herlach DM, Eckler K, Karma A, Schwarz M (2001) Mater Sci Eng A 304–306:20